Bioorganic Chemistry 77 (2018) 252–262

Contents lists available at ScienceDirect

Bioorganic Chemistry

journal homepage: www.elsevier.com/locate/bioorg

Synthesis, biological evaluation and molecular modeling studies of phenyl-/benzhydrylpiperazine derivatives as potential MAO inhibitors

Bhupinder Kumar [a], Sheetal [a], Anil K. Mantha [b], Vinod Kumar [a,*]

[a] Laboratory of Organic and Medicinal Chemistry, Department of Pharmaceutical Sciences and Natural Products, Central University of Punjab, Bathinda, Punjab 151001, India
[b] Department of Animal Sciences, School of Basic and Applied Sciences, Central University of Punjab, Bathinda, Punjab, India

ARTICLE INFO

Article history:
Received 12 October 2017
Revised 7 January 2018
Accepted 12 January 2018
Available online 16 January 2018

Keywords:
MAO inhibitor
Phenylpiperazine
1-Benzhydrylpiperazine
Cytotoxicity
Neurological disorders

ABSTRACT

Monoamine oxidase inhibitors (MAOIs) are potential drug candidates for the treatment of various neurological disorders like Parkinson's disease, Alzheimer's disease and depression. In the present study, two series of 4-substituted phenylpiperazine and 1-benzhydrylpiperazine (**1**–**21**) derivatives were synthesized and screened for their MAO-A and MAO-B inhibitory activity using Amplex Red assay. Most of the synthesized compounds were found selective for MAO-B isoform except compounds **3**, **7**, **8**, **9** and **13** (MAO-A selective) while compound **11** was non-selective. In the current series, compound **12** showed most potent MAO-B inhibitor activity with IC_{50} value of 80 nM and compound **7** was found to be most potent MAO-A inhibitor with IC_{50} value of 120 nM and both the compounds were found reversible inhibitors. Compound **8** was found most selective MAO-A inhibitor while compound **20** was found most selective inhibitor for MAO-B isoform. In the cytotoxicity evaluation, all the compounds were found non-toxic to SH-SY5Y and IMR-32 cells at 25 μM concentration. In the ROS studies, compound **8** (MAO-A inhibitor) reduced the ROS level by 51.2% while compound **13** reduced the ROS level by 61.81%. In the molecular dynamic simulation studies for 30 ns, compound **12** was found quite stable in the active cavity of MAO-B. Thus, it can be concluded that phenyl- and 1-benzhydrylpiperazine derivatives are promising MAO inhibitors and can act as a lead to design potent, and selective MAO inhibitors for the treatment of various neurological disorders.

1. Introduction

Monoamine oxidase (MAO, EC 1.4.3.4) is a flavin adenine dinucleotide (FAD)-containing outer mitochondrial membrane-bound enzyme found in the brain in neuronal, glial, and other cells [1] and also in periphery. FAD co-factor covalently bound to MAO at cysteine residue by an 8-alpha (s-cysteinyl) riboflavin linkage. MAO regulates the levels of biogenic and xenobiotic amines in the brain and in the peripheral tissues by catalyzing their oxidative deamination [2]. It acts as a catalytic agent in the oxidative deamination of various monoamines including serotonin, dopamine, histamine, adrenaline and noradrenaline. MAO enzyme exists in two isoforms, MAO-A and MAO-B [3] and these two isoforms have sequence similarity of around 73% but vary in their substrate specificity and inhibitor selectivity. MAO-A deaminates serotonin and is inhibited by clorgyline whereas MAO-B deaminates benzylamine and 2-phenylethylamine and is inhibited by (R)-deprenyl [4,5]. Iproniazid, an anti-tuberculosis drug showing mood elevation in depressed patients, was the first MAO inhibitor used in the treatment of depression [6]. It was followed by imipramine, isocarboxazid, phenelzine, tranylcypromine and propargylamines [7,8]. All of these drugs were non-selective and irreversible MAO inhibitors and were associated with number of side effects such as cheese effect, serotonin syndrome and lethal drug-drug interactions. Thus, new generations of MAO inhibitors were developed which were reversible and selective for one of the MAO isoform and devoid of many side effects [9,10]. Now, the MAO enzyme has been recognized as an important and attractive drug target for the treatment of various neurogenic disorders. Recent reports on the neuroprotective and neuro rescue potential [11,12] of MAO inhibitors have generated enormous interests for exploring their role in the treatment/management of various neurological disorders.

Piperazine is one the most promising heteroaromatic nucleus and integral part in most of the psychoactive compounds [13,14]. A number of phenylpiperazine derivatives have been synthesized and screened for their MAO inhibition potential and their role in the management of Parkinson's disease, Alzheimer's disease and depression. Pessoa-Mahana et al. [15] reported 4-arylpiperazine derivatives (A, Fig. 1) of moclobemide as new type of

* Corresponding author.
E-mail address: vinod.kumar@cup.edu.in (V. Kumar).

https://doi.org/10.1016/j.bioorg.2018.01.020
0045-2068/

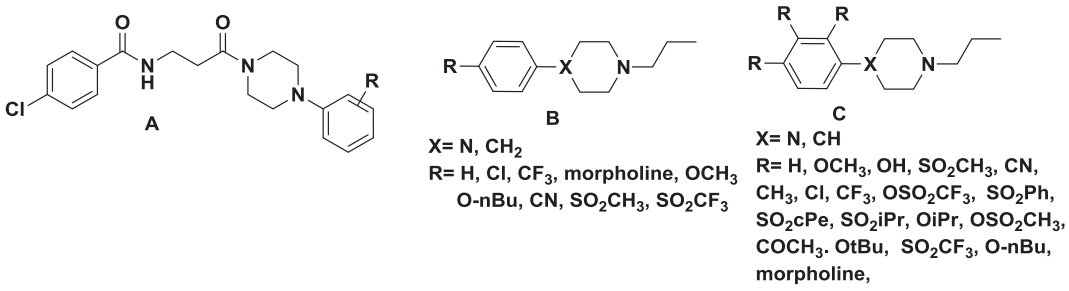

Fig. 1. Some piperazine derivatives reported as potent MAO inhibitors.

antidepressants showing MAO-A inhibitory effect and affinity towards 5-HT1$_A$. Similarly, *para*-substituted 4-phenylpiperidines and 4-phenylpiperazines (B, Fig. 1) have been synthesized and evaluated as monoamine oxidase inhibitors. It was found that *para* substituent with low dipole moment increases affinity to MAO-A, while substituent with high dipole moment have weak affinity. MAO-B affinity of the ligands was modulated by the bulk of *para*-substituent and in general hydrophobic substituents resulted in compounds with high MAO-B affinity [16]. Recently monosubstituted 4-phenylpiperidines and 4-phenylpiperazines (C, Fig. 1) have been reported [17] which showed strong correlation between the levels of striatal DOPAC and the affinity to dopamine D_2 receptor subtype and MAO-A isoform. From these reports, it can be concluded that small molecules with piperazine nucleus displayed high MAO inhibitory potency. Thus, in the current research article, we have synthesized phenylpiperazine and benzhydrylpiperazine derivatives and these were evaluated for MAO inhibitor potential using Amplex® Red assay. Most of the compounds displayed very good inhibitory activities against MAO enzyme when compared with the standard inhibitors. Molecular modeling studies were performed and it was found that the synthesized compounds fitted well in the active cavity of the MAO enzyme. In addition, these compounds were evaluated for reversibility, cytotoxicity and ROS inhibition potential and it is expected that these compounds might act as multifunctional agents.

2. Results and discussions

2.1. Chemistry

2.1.1. Synthetic schemes

Scheme 1 describe the synthesis of benzoyl- or phenylsulfonyl derivatives (**1**–**13**) of piperazine while Scheme 2 describe the reaction of appropriately substituted phenyl derivatives for the synthesis of the target compounds **14**–**21** (phenyl- or benzhydrylpiperazines).

2.2. Biological results

2.2.1. hMAO inhibition activity

The MAO inhibition potential of the phenylpiperazine and 1-benzhydrylpiperazine derivatives (**1**–**21**) was evaluated using recombinant human MAO-A, MAO-B enzymes (purchased from Sigma Aldrich) and Amplex® Red assay kit through fluorimetric method [18]. The synthesized compounds were separately evaluated for their inhibitory potential against MAO-A and MAO-B enzymes and majority of the compounds displayed inhibitory activities in sub-micromolar range. Most of the compounds were found selective for MAO-B isoform except compounds **3, 7, 8, 9** and **13** which showed selectivity for MAO-A isoform. Compound **11** was found nonselective for either of the MAO isoforms. Compound **1** (Table 1), having two unsubstituted phenyl groups, showed MAO-B inhibition activity with IC_{50} value of 0.41 ± 0.02 μM with selectivity index (SI) of more than 122 folds over MAO-A. Similarly, compound **20** (Table 1) with hydrophobic anthracene moiety was found most selective towards MAO-B isoform with SI of more than 150 folds over MAO-A and displayed IC_{50} value of 0 .33 ± 0.09 μM. In this series, compound **12** (Table 1) was found most potent MAO-B inhibitor with IC_{50} value of 0.08 ± 0.003 μM, about two times more potent than the standard inhibitor pargyline (entry 23, Table 1). On the other hand, compound **7** (Table 1) with a 4-tertbutyl substituent on the benzene ring was found most potent MAO-A inhibitor with an IC_{50} value of 0.12 ± 0.06 μM. Compound **8**, with a chloro and two methyl groups as substituents, was found most selective (>14 folds) towards MAO-A (IC_{50} = 0.32 ± 0.11 μM) over MAO-B (IC_{50} = 4.53 ± 0.15 μM). As evident from the Table 1,

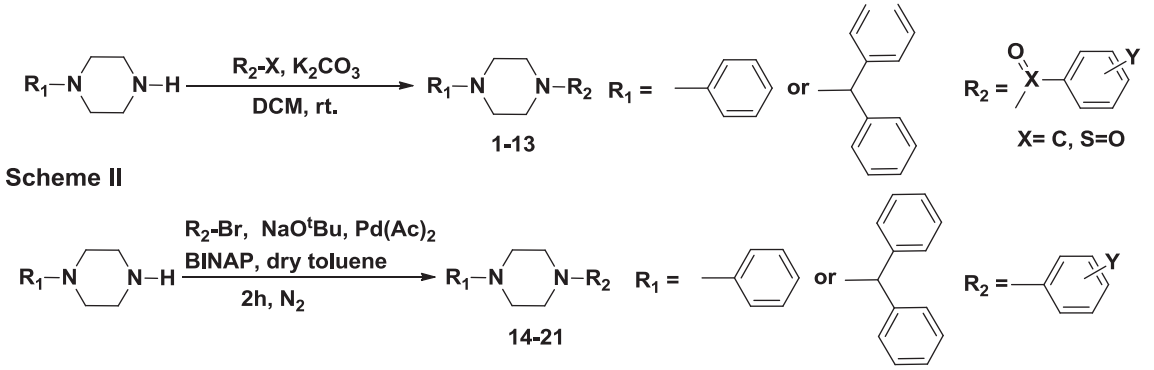

Scheme 1.

Table 1
MAO inhibition profile of the synthesized compounds **1–21** expressed as IC_{50} μM.

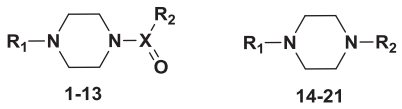

Entry name	R_1	R_2	X	IC_{50} values (mean ± S.E. μM)		SI	Docking score of MAO-A	Docking score of MAO-B
				MAO-A	MAO-B			
1	C_6H_5	C_6H_5	C	>50[a]	0.41 ± 0.02	>122	−7.58	−10.26
2	C_6H_5	4-$OCH_3C_6H_4$	C	>50[a]	3.21 ± 0.11	15.57	−4.74	−9.36
3	C_6H_5	4-$CH_3C_6H_4$	C	2.90 ± 0.09	5.19 ± 0.21	0.56	−7.73	−9.42
4	C_6H_5	2-$NO_2C_6H_4$	S=O	>50[a]	15.17 ± 0.29	>3	−7.45	−8.45
5	C_6H_5	4-Cl-2,5-$(CH_3)_2C_6H_2$	S=O	6.14 ± 1.02	1.54 ± 0.03	3.99	−6.77	−7.51
6	C_6H_5	4-TertbutylC$_6H_4$	S=O	>50[a]	0.96 ± 0.03	>52	−3.37	−3.03
7	-Benzhydryl	4-TertbutylC$_6H_4$	S=O	0.12 ± 0.06	0.61 ± 0.04	0.19	−7.53	−4.32
8	-Benzhydryl	4-Cl-2,5-$(CH_3)_2C_6H_5$	S=O	0.32 ± 0.11	4.53 ± 0.15	0.07	−5.86	−6.46
9	-Benzhydryl	4-$NO_2C_6H_4$	S=O	0.46 ± 0.13	0.77 ± 0.05	0.59	−4.43	−7.68
10	-Benzhydryl	4-$CH_3C_6H_4$	S=O	1.82 ± 0.34	1.04 ± 0.32	1.75	−4.19	−7.62
11	-Benzhydryl	2-$NO_2C_6H_4$	S=O	0.47 ± 0.08	0.49 ± 0.02	0.95	−5.34	−5.02
12	-Benzhydryl	C_6H_5	C	1.02 ± 0.16	0.08 ± 0.003	12.75	−7.41	−8.69
13	-Benzhydryl	4-$NO_2C_6H_4$	C	0.83 ± 0.25	6.41 ± 0.17	0.13	−6.76	−10.22
14	C_6H_5	C_6H_5	–	>50[a]	5.81 ± 0.22	>8.60	−7.45	−9.62
15	C_6H_5	3-Quinoline	–	>50[a]	0.77 ± 0.13	>65	−7.79	−9.26
16	C_6H_5	1-Naphthalene	–	>50[a]	0.98 ± 0.18	>51	−7.65	−11.07
17	-Benzhydryl	—$CH_2C_6H_5$	–	4.73 ± 1.09	0.61 ± 0.04	7.75	−7.67	−7.75
18	-Benzhydryl	C_6H_5	–	3.41 ± 0.17	0.65 ± 0.05	5.24	−8.65	−9.72
19	-Benzhydryl	3-Quinoline	–	4.48 ± 0.32	0.35 ± 0.11	12.80	−6.06	−11.47
20	-Benzhydryl	9-Anthracene	–	>50[a]	0.33 ± 0.09	>150	[b]	−10.81
21	-Benzhydryl	1-Naphthalene	–	>50[a]	0.50 ± 0.01	>100	−5.83	−11.55
22	**Clorgyline**		–	4.39 ± 1.02 nM	–	–	–	–
23	**Pargyline**		–	–	0.15 ± 0.02	–	–	–

SI = IC_{50} of MAO-A/IC_{50} of MAO-B.
[a] Inactive or showed less than 50% inhibitory activity at 50 μM concentration and precipitated at higher concentrations.
[b] Unable to enter MAO-A active site

all the compounds showed potent MAO inhibition activities. Thus, consistently with the other literature reports [16], we found that the compounds with polar and electron donating substituents such as compound **8** have a high affinity for MAO-A isoform while compounds with hydrophobic bulky groups showed affinity towards MAO-B isoform (compounds **20** and **21**).

2.2.2. Reversibility studies

Most of the first-generation MAO inhibitors were irreversible in nature and were responsible for a number of side effects that include cheese effect, drug-food interactions and drug-drug interactions. Thus, reversibility is an important characteristic of MAO inhibitors and frequently hunted in the designing and development of new MAO inhibitors.

The most potent compounds **7** (MAO-A) and **12** (MAO-B) and other four compounds i.e. **1, 8, 13** and **20** which showed high selectivity for either of the MAO isoform, were evaluated for reversibility using reported protocols [19,20]. Compound **7** and **13** were found reversible inhibitors of MAO-A isoform and the activity of MAO-A enzyme could be recovered up to 67.32% and 63.56% respectively (Fig. 2). The compound **8** (MAO-A inhibitor) was found irreversible inhibitor as there was no significant recovery in the MAO-A activity (8.28%) after the addition of substrate. In the reversibility studies on MAO-B isoform, all the tested compounds (compound **1**, **12** and **20**) were found reversible inhibitors. The most potent MAO-B inhibitor i.e. compound **12** showed enzymatic activity recovery up to 78.45% in the reversibility studies. The compounds **1** and **20** (MAO-B inhibitors) also showed recovery in the MAO-B activities up to 60.12% and 98.08% respectively (Fig. 3). Both the standard inhibitors i.e. clorgyline (MAO-A) and pargyline (MAO-B) did not show any recovery in the activity after treatment with the substrate, thus confirming their irreversible character as reported in the literature.

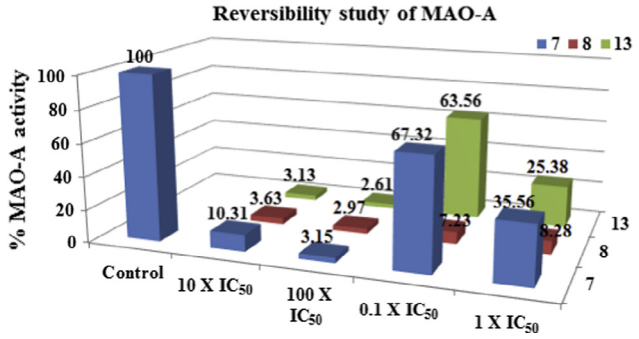

Fig. 2. Reversibility studies of compound **7**, **8** and **13** on MAO-A isoform. Compounds **7** and **13** were found reversible while compound **8** was found irreversible.

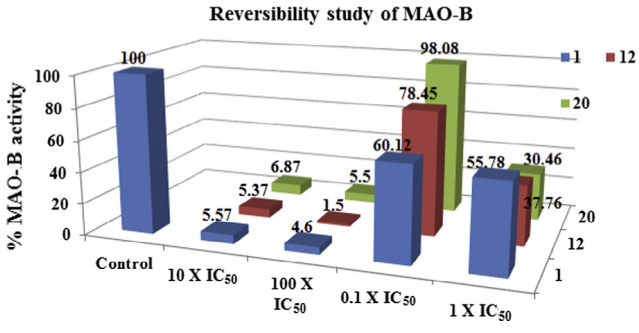

Fig. 3. Reversibility studies of compound **1**, **12** and **20** with the MAO-B isoform. All the three compounds were found reversible inhibitors of MAO-B isoform.

2.2.3. Cytotoxicity studies

Cytotoxicity of the most potent and selective MAO inhibitors (compounds **1**, **7, 8, 12**, **13** and **20**) was evaluated against SH-SY5Y and IMR-32 cells. The cells were treated with 25 μM concentrations of the test compounds for 24 h and 48 h and the results were compared with the control experiments. For compounds **1**, **12** and **20** (MAO-B inhibitors), cell viability up to 117%, 88%, 87% in SH-SY5Y cells and 104%, 95%, 97% in IMR-32 cells, respectively, have been observed. Similarly, for compounds **7, 8** and **13** (MAO-A inhibitors) cells viability up to 98%, 93%, 86% in SH-SY5Y cells and 94%, 91%, 87% in IMR-32 cells, respectively, was observed (Fig. 4). Hence, in the cytotoxicity studies it was found that this series of compounds do not affect cell division significantly and it can be concluded that compounds were non-toxic to the tissue cells.

2.2.4. ROS inhibition studies

It is a well-known fact that MAO mediated oxidative metabolism of monoamines lead to the production of H_2O_2 as a byproduct [21,22]. Subsequently, H_2O_2 get converted into free radicals through Fenton's reaction and contribute to the oxidative stress. Uncontrolled increase in the concentrations of these free radicals, initiate free radical-mediated chain reactions, that causes oxidative damage to the cell membranes, lipid peroxidation and DNA strand breakdown. Thus, prevention of ROS generation along with MAO inhibition is also an important strategy to prevent neurotoxicity in neurodegenerative diseases.

Intracellular levels of ROS were determined using non-fluorescent compound 2,7-dichlorofluorescein diacetate (DCF-DA). The SH-SY5Y cells were treated with two different concentrations (0.1 μM and 1 μM) of the test compounds for 24 h and 48 h time intervals. In this study, it has been found that compound **1, 12** and **20** (MAO-B inhibitors) did not show any significant reduction in the intracellular ROS levels. The compound **1** lowered the ROS levels by 11% after 24 h and by 20% after 48 h as compared to the control (100%) while compound **20** showed reduction in ROS levels by 27% after 48 h of treatment. Most potent MAO-B inhibitor **12** reduced the intracellular ROS level by 25% only (Fig. 5). However, compounds **7**, **8** and **13** (MAO-A inhibitors) significantly reduced the intracellular ROS levels after 24 h treatment. The compound **7** reduced the ROS levels by 56.44%, **8** by 51.2% and compound **13** reduced the ROS levels by 61.81% at 1 μM and 24 h treatment.

2.2.5. Molecular docking studies

To know about the orientation of the ligands and their interactions at the receptor site, all the compounds were docked at the respective active sites of the receptor. Using Maestro 11.1 (Schrödinger LLC) software, compounds were docked at the hMAO-A (PDB ID- 2BXR) and hMAO-B (PDB ID-2BYB) [23] crystal structures, respectively, imported from the protein data bank. The docking procedures were first validated by accurately redocking the co-crystallized ligands into the MAO models. The docking score of all the compounds are described in Table 1 and docking poses of the most active compounds are displayed in Figs. 6 and 7.

In case of compound **7** and **8** (most potent and selective MAO-A inhibitors) the benzhydrylpiperazine moiety was positioned towards the FAD cofactor (Fig. 6A and C) and substituted sulfonyl group oriented towards the hydrophobic entrance cavity. The benzhydrylpiperazine moiety forms the π-π stacking with Tyr69, Tyr197, Tyr407, Tyr444 lining hydrophobic pocket of the MAO-A active site. The substituted sulfonyl moiety was oriented towards the entrance of the MAO-A active site lined by residues Leu97, Met324, Ile325 and Thr336 (Fig. 6B and D). In case of **13**, orientation of the compound at the active site get reversed. The benzhydryl moiety was oriented towards the entrance cavity while *p*-nitrobenzene moiety aligned towards FAD cofactor (Fig. 6E). Nitro group of the compound **13** formed hydrogen bonds with Thr73 and Arg206 (Fig. 6F).

The active site of MAO-B comprises an entrance cavity and substrate cavity. Most important residues of the active site of MAO-B include aromatic amino acid residues such as Tyr435 and Tyr188, which forms the π-π stacking with the aromatic rings of the ligand. Both entrance and substrate cavities are relatively lipophilic and Ile199 residue effectively serves as a gate between these cavities. The docking orientations of the compound **1, 12** and **20** (most potent and selective MAO-B inhibitors) showed that the piperazine moiety in all the compounds interacts with the Ile199 (Fig. 7) residues keeping it in open gate conformations. Thus it is concluded that all of these compounds might block the entrance cavity and inhibit entry of the substrate to the substrate cavity. Both entrance and substrate cavities are lipophilic and compounds showed hydrophobic interactions with Tyr60, Phe103, Tyr188, Tyr326, Phe343 and Tyr435 residues lining hydrophobic cavity of MAO-B. All the three inhibitors showed π-π stacking with Tyr435 and Tyr188 at the active site. Another interesting finding during the docking studies was that compound **20** was unable to enter the active site of MAO-A isoform.

2.2.6. Molecular dynamic simulation studies

Molecular dynamic simulations (MD) were performed to study protein–ligand interactions and to determine the thermodynamic stability of docked compounds at the active pocket MAO enzyme.

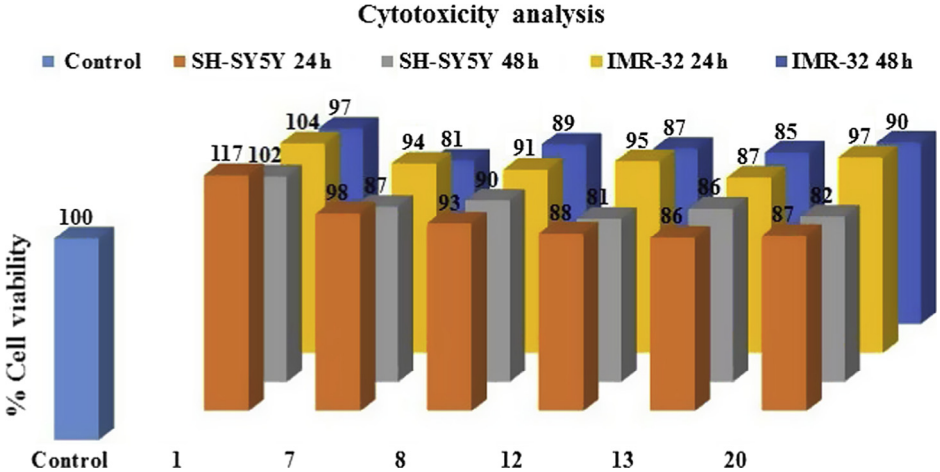

Fig. 4. Cytotoxicity studies of compound **1**, **7**, **8**, **12**, **13** and **20** on the SH-SY5Y and IMR-32 cells. All the tested compounds were found non-toxic to the cells.

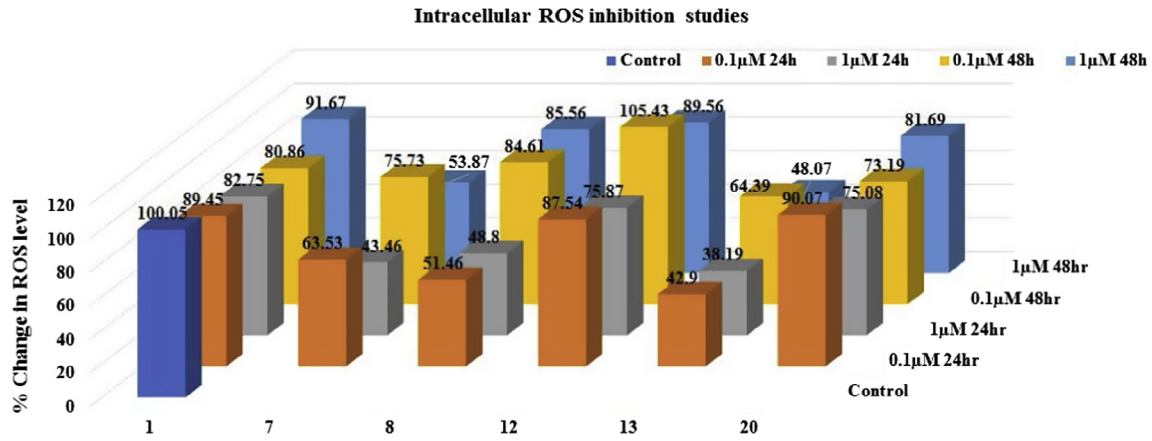

Fig. 5. ROS inhibition studies of the tested compounds (compound **1**, **7**, **8**, **12**, **13** and **20**) on SH-SY5Y cells. Compound **1**, **12** and **20** (MAO-B inhibitors) did not show any significant reduction in the intracellular ROS levels while compounds **7**, **8** and **13** (MAO-A inhibitors) significantly reduced the intracellular ROS levels after 24 h treatment.

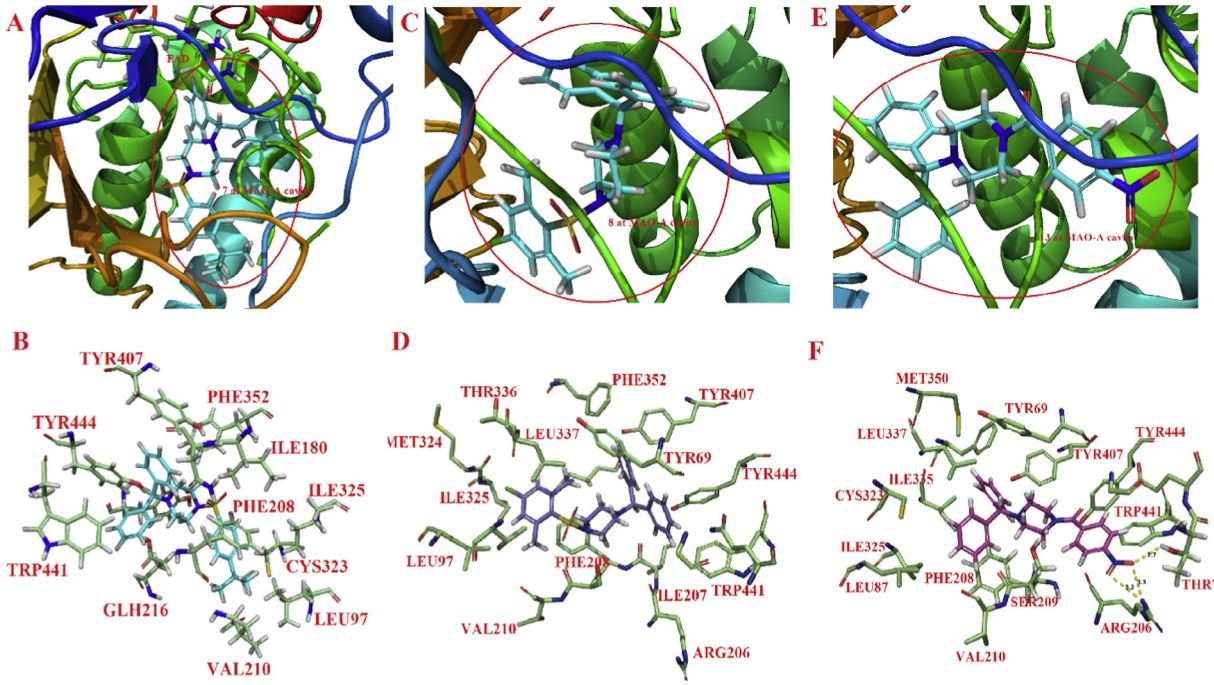

Fig. 6. (A) Orientation of compound **7** at MAO-A cavity with FAD cofactor; (B) Binding interactions of compound **7** (cyan) with the active site residues of MAO-A; (C) Orientation of compound **8** at the MAO-A cavity with FAD cofactor, (D) Binding interactions of compound **8** (blue) with the active site residues of MAO-A; (E) Orientation of compound **13** at the MAO-A cavity with FAD cofactor; and (D) Binding interactions of compound **13** (purple) with the active site residues of MAO-A. (For interpretation of the references to colour in this figure legend, the reader is referred to the web version of this article.)

Thus a protein–ligand docked complex of the most active compound (**12**) with MAO-B was used for MD simulations. The MD simulation studies were conducted for 30 ns and interaction pattern of the test compound with different amino acids was analyzed. Ile199 and Tyr326 residues separate the two cavities of MAO-B and these residues play crucial role in imparting structural preference for MAO-B selective ligands. From the bar diagram of protein ligand contacts (Fig. S1) it has been observed that compound 12 showed maximum interactions with Ile199 and Tyr326. Nitrogen atom of piperazine ring showed water bridges and hydrogen bonding while piperazine ring showed hydrophobic interactions with Ile199 residue. Compound **12** was found to bind at the same site keeping residue Ile199 in "open gate" conformation. In the MD simulation studies (30 ns) compound **12** was found stable (RMSD less than 3 Å) in the hydrophobic pocket of MAO-B lined by residues Tyr60, Leu164, Tyr326 and Tyr398. Although some new interactions were also observed. Nitrogen atom of **12** form hydrogen bond through water bridge and oxygen atom of carbonyl group form hydrogen bond with residue Tyr398 (Fig. 8). Compound **12** also showed π-π stacking with Tyr60 (Fig. S1). RMSD of **12** showed fluctuations in between 1.6 and 2.0 Å. After 7 ns compound **12** was found most stable (Fig. S2) in the binding pocket. Protein RMSD was also found to be less than 3 Å, well within the acceptable limits.

2.2.7. Physicochemical properties

In order to assess the drug-like characteristics of the most active compounds, various physicochemical parameters of these compounds have been evaluated using Qikprop application of Schrodinger suit. The molecular weight of all the compounds is less than 500 and ClogP values of all the compounds except **7** and **20,** was found less than 5, in agreement with the Lipinski's rule of 5

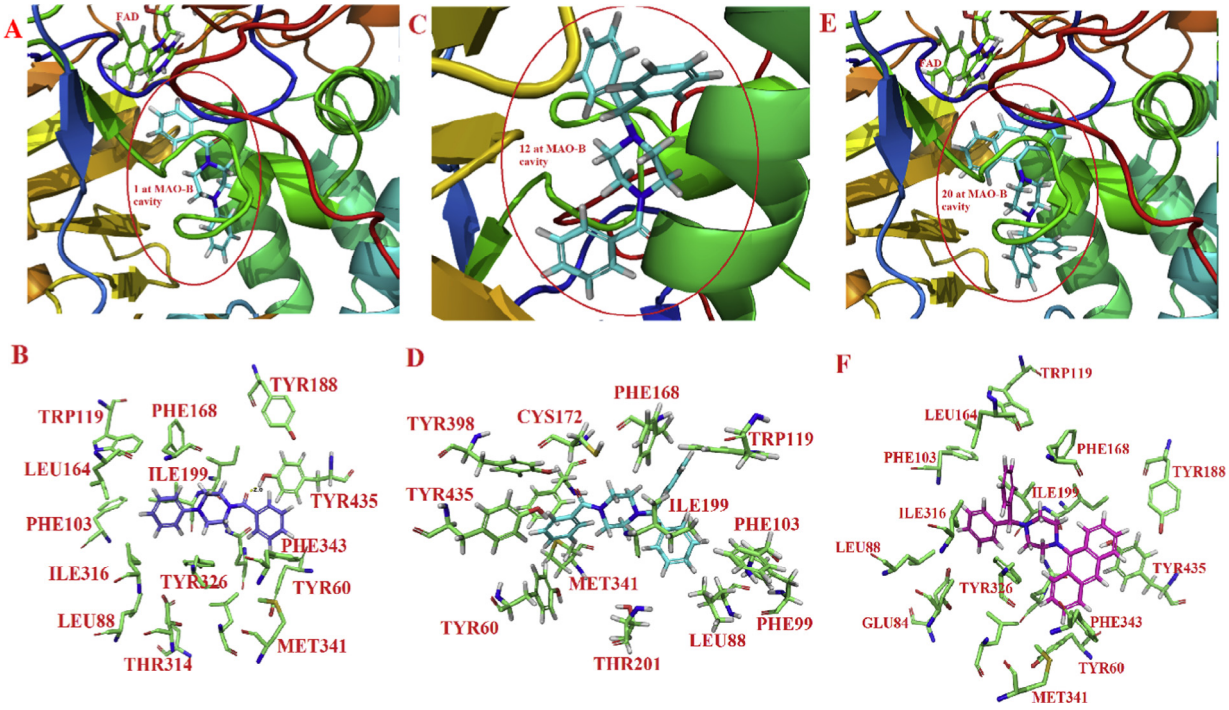

Fig. 7. (A) Orientation of compound **1** at the MAO-B cavity with FAD cofactor; (B) Binding interactions of compound **1** (blue) with the active site residues of MAO-B; (C) Orientation of compound **12** at MAO-B cavity with FAD cofactor; (D) Binding interactions of compound **12** (cyan) with the active site residues of MAO-B; (E) Orientation of compound **20** at the MAO-B cavity with FAD cofactor; and (F) Binding interactions of compound **20** (purple) with active site residues of MAO-B. (For interpretation of the references to colour in this figure legend, the reader is referred to the web version of this article.)

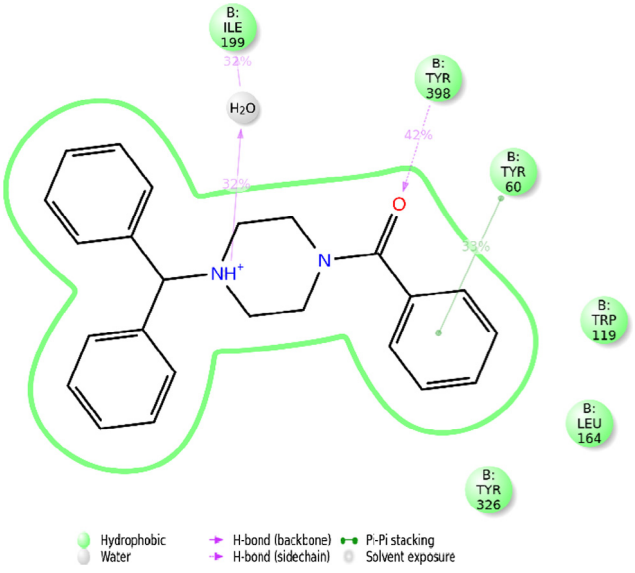

Fig. 8. Interactions of compound **12** in the active cavity of MAO-B post MD (30 ns) simulation studies.

for drug-likeness. All the test compounds showed QPlogBB value in the range of −0.97 to 0.32, which is a suitable range for the crossing of blood-brain barrier. From these studies, it can be concluded that the most active compounds (compounds **1**, **7**, **8**, **12**, **13** and **20**) displayed drug-like characteristics including blood-brain barrier permeability (see Table 2).

2.2.8. SAR studies

In the current studies, two different series of compounds (Sr. No 1 to 13 and 14 to 21; Table 1) were evaluated against MAO-A and MAO-B isoforms. Most of the compounds showed MAO inhibitory activities with IC_{50} values in low to the sub-micro molar range. The first series of compounds (**1**–**13**; Table 1) consist 4-substituted benzoyl or phenylsulfonyl groups (R_2) attached to the phenyl- and benzhydrylpiperazine (R_1). In the second series (14 to 21; Table 1), an optionally substituted aromatic ring was attached to the pheny-/1-benzhydrylpiperazine ring. Compound **1** with an unsubstituted benzoyl group and unsubstituted phenyl ring exhibited very high SI (122 folds) towards MAO-B isoform with an IC_{50} value of 0.41 ± 0.02 μM. Methoxy (compound **2**) or methyl (compound **3**) substituents on the benzoyl ring has reduced the potency and selectivity for MAO-B isoform. However, when phenyl group (R_1 substituent, Table 1) in compound **1** is replaced with the benzhydryl group, it resulted in the most potent MAO-B inhibitor (compound **12**) with IC_{50} value of 0.08 ± 0.003 μM and SI of more than 12. 4-Nitro substitution on the phenyl ring of **12**, resulted in compound **13** with reduced potency for MAO-B but more selectivity (8 folds) for MAO-A isoform. In general replacement of benzoyl groups with phenylsulfonoyl groups, resulted in increased potency for MAO-A isoform and 4-tertbutyl substituted phenylsulfonyl derivative (compound **7**) was found most potent MAO-A inhibitor with an IC_{50} value of 0.12 ± 0.06 μM. Similarly, 4-chloro-2,5-dimethyl substituted derivative (compound 8) exhibited high SI (more than 14 folds) for MAO-A isoform with an IC_{50} value of 0.32 ± 0.06 μM. All the compounds of the second series showed moderate to high selectivity for MAO-B isoform. Biphenyl substituted piperazine nucleus (compound **14**) displayed 8 folds selectivity for MAO-B. Bulkier and hydrophobic groups like quinoline (compound **15**) and naphthalene (compound **16**) showed more selectivity for MAO-B isoform. Compound **20** with a hydrophobic anthracene group exhibited more than 150 folds selectivity for MAO-B with an IC_{50} value of 0.33 ± 0.09 μM. High selectivity of these bulkier compounds for MAO-B isoform may be attributed to the large entrance cavity of MAO-B in comparison to MAO-A isoform. The active site of MAO-B can better accommodate these

Table 2
Physicochemical properties of some of the potent and selective MAO inhibitors.

Compound number	Mol. Wt.	Log P	HB donor	HB acceptor	% Human oral absorption	QPlogBB (Optimum range −3.0 to 1.2)	BBB permeability predicted
1	266.342	3.571	0	4	100	0.161	+ve
7	448.622	5.206	0	7	95.78	−0.003	+ve
8	455.013	4.993	0	7	100	0.316	+ve
12	356.466	4.424	0	5	100	0.35	+ve
13	401.464	3.77	0	6	87	−0.738	+ve
20	428.576	7.108	0	3	100	−0.972	+ve

+ve = blood-brain barrier permeable; −ve = no permeability to the blood-brain barrier.

non-polar ligands and hydrophobic cavity stabilizes it through lipophilic interactions. In the molecular docking studies, it has been observed that compound **20** was unable to enter the active site of MAO-A.

3. Conclusion

A total of 21 phenyl- or benzhydrylpiperazine derivatives were designed, synthesized and screened for their MAO inhibition potential using Amplex® Red based assay. Most of the synthesized compounds displayed good inhibition activity for MAO enzyme, comparable with standard inhibitors. Amongst these compounds, compound **1** and **20** were found most selective MAO-B inhibitors while compound **8** and **13** were found selective MAO-A inhibitors. Compound **12** displayed most potent MAO-B inhibitor activity with an IC_{50} value of 80 nM. Similarly compound **7** was found most potent MAO-A inhibitor with an IC_{50} value of 120 nM. In the reversibility studies, all the active and highly selective compounds were found reversible inhibitors of MAO enzyme except compound **8**. In cytotoxicity studies, all the compounds were found safe against SH-SY5Y and IMR-32 cells. In the ROS inhibition studies, compound **7**, **8** and **13** (MAO-A inhibitors) significantly reduced the intracellular ROS levels after 24 h treatment. From molecular docking studies, it has been found that the bulkier and hydrophobic groups were not entering into the smaller MAO-A cavity but showed good binding affinities at the MAO-B cavity. These findings were consistent with the selectivity results obtained for most of the compounds with the bulkier groups (compound **6**, **15**, **16**, **20** & **21**). In the MD simulation studies (30 ns), compound 12 was found stable in the binding pocket of MAO-B. Thus, it is envisaged that some of the promising compounds in the current piperazine based series especially compound **7** and **12** can act as lead compounds for the development of effective and potent MAO inhibitors for the treatment of various neurological disorders.

4. Experimental

4.1. Material and methods

All the chemicals and reagents used for the synthesis were purchased from Sigma-Aldrich, Loba-Chemie Pvt. Ltd. and S.D. Fine Chemicals are used without further purification. Thin layer chromatography was done on glass silica plates with silica gel G as the adsorbent. Ethyl acetate: petroleum ether (1:1), (2:3) and methanol: chloroform (0.5% methanol in chloroform with 2–3 drops of ammonium hydroxide) mixtures were used as a solvent system for the chromatographic purification of compounds. Spots were visualized under UV light and iodine chamber. Mass spectra were recorded on GC–MS (ESI), Central Instruments Laboratory (CIL), Central University of Punjab, Bathinda. The ^{1}H and ^{13}C NMR of the compounds were recorded on JEOL or Bruker Advance II instrument at 400 MHz frequency, in $CDCl_3$ or DMSO and TMS (δ = 0) as an internal standard at IIT Ropar, and Punjab University, Chandigarh. The chemical shifts are reported in parts per million (δ) downfield from the signal of tetramethylsilane added to the deuterated solvent. Spin multiplicities are given as s (singlet), b (broad), d (doublet), dd (double doublet), t (triplet), q (quartet) or m (multiplet). Melting points were recorded with Stuart SMP30 melting point apparatus and are uncorrected. For MAO inhibition studies Amplex® Red MAO kit was purchased from Molecular Probes (Invitrogen), Life technologies, India. Recombinant hMAO-A and hMAO-B enzymes were purchased from Sigma-Aldrich. For absorption studies UV–VIS spectrophotometer of Shimadzu was used. Fluorescence studies were recorded using Biotek Microplate reader. Molecular modeling studies were carried out using Maestro 11.1 (Schrödinger LLC) and ChemBio Draw Ultra-12 installed on operating system Window 7 and centos 6.5 at HP-2800 workstation with configuration of intel (R) Xenon (R) X5660 @2.80 GHz, 2.789 GHz (2 processors).

4.2. Chemistry

4.2.1. General procedure for the synthesis of piperazine derivatives from 1 to 13

The first series of compounds were synthesized using reaction Scheme 1. In 100 mL RBF, 1-substituted piperazine (0.01 mmol, 1 eq.), potassium carbonate (0.015 mmol, 1.5 eq.) was dissolved in 15 mL dichloro methane (DCM). The reaction mixture was kept under stirring at 0 °C for 10 min. To it substituted sulfonyl or benzoyl chloride (0.015 mmol, 1.5 eq.) was added portion wise in 5-min time. The reaction was brought to room temperature and kept on stirring for 6–8 h. The completion of the reaction was confirmed by TLC. DCM was evaporated on rota-evaporator and to the residue water added; the aqueous layer was extracted with ethyl acetate. The organic layer was washed with brine, passed through sodium sulphate and removed on rota-evaporator. The products were purified using column chromatography on silica gel (60–120).

1. Phenyl (4-phenylpiperazin-1-yl)methanone [24,25]

Yield 62%; **IR (KBr** cm^{-1}**):** 3329 (NH stretch), 2212 (CN stretch), 1683 (C=O stretch), 1830.10 (C=C stretch).**^{1}H NMR** (400 MHz, $CDCl_3$, TMS = 0) δ: 3.25 (4H, t, *J* = 4 Hz), 3.65 (4H, t, *J* = 8 Hz), 6.95 (2H, d, *J* = 8 Hz), 7.25 (1H, t, *J* = 8 Hz), 7.30 (2H, d, *J* = 8 Hz), 7.43 (1H, t, *J* = 8 Hz), 7.60 (2H, d, *J* = 4 Hz), 8.08 (2H, d, *J* = 8 Hz); **^{13}C NMR** (100 MHz, $CDCl_3$, TMS = 0) δ: 130.0, 129.4, 128.7, 127.2, 117.0, 49.12, 47.52. **ESI-MS *m/z*:** 266.

2. (4-Methoxyphenyl)(4-phenylpiperazin-1-yl)methanone [26,27]

Yield 56%; **IR (KBr** cm^{-1}**):** 1683 (C=O stretch), 1239 (CN stretch), 2961 (CH stretch), 1310 (CO stretch), 1298.15 (CC stretch) 1830.10 (C=C stretch),**^{1}H NMR** (400 MHz, $CDCl_3$, TMS = 0) δ: 3.13 (3H, s,), 3.78 (4H, t, *J* = 8 Hz), 3.82 (4H, t, *J* = 8 Hz), 6.69 (2H, d, *J* = 4 Hz), 7.23 (1H, t, *J* = 8 Hz), 7.36 (2H, d, *J* = 8 Hz), 7.99 (1H, d, *J* = 8 Hz), 8.03 (1H, d, *J* = 8 Hz); **^{13}C NMR** (100 MHz, $CDCl_3$, TMS = 0) δ: 171.09, 170.55, 164.66, 164.06, 162.39, 160.99, 132.94, 132.42, 129.35, 121.69, 116.88, 114.21, 113.86, 113.82, 55.6, 49.98, 47.5. **ESI-MS *m/z*:**296.

3. (4-Methylpiperazin-1-yl)(p-tolyl)methanone [28]

Yield 87%; **IR (KBr cm^{-1}):** 3329 (NH stretch), 2212 (CN stretch), 1683 (C=O stretch), 1034.68 (CC stretch). **^{1}H NMR** (400 MHz, $CDCl_3$, TMS = 0) δ: 2.31 (3H, s), 3.08 – 3.15 (4H, bd), 3.56 – 3.85 (4H, bd), 6.82–6.87 (3H, m), 7.15 (2H, d, *J* = 8 Hz), 7.18–7.23 (2H, m), 7.27 (2H, d, *J* = 8 Hz); **^{13}C NMR** (100 MHz, $CDCl_3$, TMS = 0) δ: 170.74, 151.08, 140.18, 132.69, 129.39, 129.26, 127.37, 120.77, 116.88, 50.05, 47.84, 42.28, 21.55. **ESI-MS *m/z*:** 280.

4. 1-((2-Nitrophenyl)sulfonyl)-4-phenylpiperazine

Yield 82%; **IR (KBr cm^{-1}):** 1237(CN stretch), 2988(CH stretch), 1690 (C=O stretch), 1298.15 (CC stretch) 1050.87 (S=O stretch), 1529 (NO_2 Symmetric stretch) **^{1}H NMR** (400 MHz, $CDCl_3$, TMS = 0) δ: 3.26 (4H, t, *J* = 4 Hz), 3.49 (4H, t, *J* = 8 Hz), 6.94–7.00 (3H, m), 7.26–7.30 (2H, m), 7.63–7.64 (1H, m), 7.70–7.73 (2H, m), 8.00 (1H, d, *J* = 8 Hz); **^{13}C NMR** (100 MHz, $CDCl_3$, TMS = 0) δ: 148.21, 134.06, 131.73, 131.10, 129.53, 124.33, 117.42, 49.97, 45.87 **ESI-MS *m/z***: 347.

5. 1-((4-Chloro-2,5-dimethylphenyl)sulfonyl)-4-phenylpiperazine

Yield 76%; **IR (KBr cm^{-1})**: 1231.34 (CN stretch), 2932.14 (CH stretch), 1166.13 (CC stretch) 1830.10 (C=C stretch), 942.41 (S=O stretch) **^{1}H NMR** (400 MHz, $CDCl_3$, TMS = 0) δ: 2.33 (3H, s), 2.51 (3H, s), 3.15 (4H, bd), 3.24 (4H, bd), 6.84 (3H, m), 7.18–7.20 (2H, m), 7.24 (1H, s), 7.72 (1H, s); **^{13}C NMR** (100 MHz, $CDCl_3$, TMS = 0) δ: 150.80, 139.39, 137.05, 134.39, 133.58, 133.23, 132.73, 129.41, 121.03, 117.08, 49.51, 45.39, 20.34, 19.72. **ESI-MS *m/z***: 364.

6. 1-((4-(*Tert*-butyl)phenyl)sulfonyl)-4-phenylpiperazine

Yield 85%; **IR (KBr cm^{-1}):** 1242 (CN stretch), 3069 (CH stretch), 946.58 (S=O stretch), 1166 (CC stretch), 1919 (C=C stretch) **^{1}H NMR** (400 MHz, $CDCl_3$, and TMS = 0) δ: 1.33 (9H, s), 3.22 (4H, t, *J* = 8 Hz), 3.24 (4H, t, *J* = 8 Hz), 6.87 (3H, m), 7.24 (2H, m), 7.53 (2H, d, *J* = 8 Hz), 7.69 (2H, d, *J* = 8 Hz); **^{13}C NMR** (100 MHz, $CDCl_3$, and TMS = 0) δ: 156.93, 150.79, 132.19, 129.40, 127.92, 126.23, 121.02, 117.04, 49.34, 46.21, 35.34, and 31.22 **ESI-MS *m/z***: 358.

7. 1-Benzhydryl-4-((4-(*tert*-butyl)phenyl)sulfonyl)piperazine [29]

Yield 87%; **^{1}H NMR** (400 MHz, $CDCl_3$, TMS = 0) δ: 1.37 (9H, s), 2.47 (4H, b), 3.03 (4H, b), 4.21 (1H, s), 7.14–7.17 (2H, m), 7.21–7.25 (4H, m), 7.32–7.34 (4H, m), 7.54 (2H, d, *J* = 8 Hz), 7.67 (2H, d, *J* = 8 Hz); **^{13}C NMR** (100 MHz, $CDCl_3$, TMS = 0) δ: 156.54, 142.05, 132.56, 128.64, 127.78, 127.21, 126.07, 75.81, 51.09, 46.28, 35.22, 31.15 **MS-ESI: *m/z:*** 448.

8. 1-Benzhydryl-4-((4-chloro-2,5-dimethylphenyl)sulfonyl) piperazine

Yield 85%; mp 176–178 °C, **^{1}H NMR** (400 MHz, $CDCl_3$, TMS = 0) δ: 2.37 (3H, s), 2.43 (4H, t, *J* = 5 Hz), 2.54 (3H, s), 3.14 (4H, t, *J* = 5 Hz), 4.22 (1H, s), 7.15–7.18 (2H, m), 7.23–7.26 (4H, m), 7.29(1H, s), 7.34–7.36 (4H, m), 7.71 (1H, s); **^{13}C NMR** (100 MHz, $CDCl_3$, TMS = 0) δ: 142.0, 139.01, 136.91, 134.16, 133.48, 133.04, 132.59, 128.66, 127.79, 127.23, 75.76, 51.18, 45.56, 20.32, 19.58 **HRMS**: for $C_{25}H_{27}ClN_2O_2S$, calculated $[M+H]^+$: 455.1560; observed $[M+H]^+$: 455.1548.

9. 1-Benzhydryl-4-((4-nitrophenyl)sulfonyl)piperazine

Yield 90%; mp 149–151 °C, **^{1}H NMR** (400 MHz, $CDCl_3$, TMS = 0) δ: 2.48 (4H, t, *J* = 4 Hz), 3.07 (4H, b), 4.23 (1H, s), 7.14–7.18 (2H, m), 7.21–7.25 (4H, m), 7.30–7.32 (4H, m), 7.93 (2H, d, *J* = 9 Hz), 8.39 (2H, d, *J* = 9 Hz); **^{13}C NMR** (100 MHz, $CDCl_3$, TMS = 0) δ: 150.27, 141.75, 141.67, 128.99, 128.69, 127.71, 127.31, 124.38, 75.50, 50.76, 46.36. **HRMS**: for $C_{23}H_{23}N_3O_4S$, calculated $[M+H]^+$: 438.1488; observed $[M+H]^+$: 438.1463.

10. 1-Benzhydryl-4-tosylpiperazine [29,30]

Yield 82%; **^{1}H NMR** (400 MHz, $CDCl_3$, TMS = 0) δ: 2.44–2.47 (7H, m), 3.01 (4H, b), 4.21 (1H, s), 7.12–7.17 (2H, m), 7.20–7.24 (4H, m), 7.30–7.35 (6H, m), 7.62–7.64 (2H, m); **^{13}C NMR** (100 MHz, $CDCl_3$, TMS = 0) δ: 143.64, 142.06, 132.51, 129.70, 128.62, 127.94, 127.76, 127.19, 75.69, 50.97, 46.34, 21.60 **MS-ESI: *m/z:*** 406.

11. 1-Benzhydryl-4-((2-nitrophenyl)sulfonyl)piperazine [31]

Yield 83%; **^{1}H NMR** (400 MHz, $CDCl_3$, and TMS = 0) δ: 2.46 (4H, t, *J* = 4 Hz), 3.30 (4H, t, *J* = 4 Hz), 4.24 (1H, s), 7.15–7.19 (2H, m), 7.23–7.27 (4H, m), 7.35–7.36 (4H, m), 7.57–7.59 (1H, m), 7.63–7.71 (2H, m), 7.90–7.93 (1H, m); **^{13}C NMR** (100 MHz, $CDCl_3$, and TMS = 0) δ: 148.59, 141.95, 133.75, 131.44, 130.97, 130.79, 128.69, 127.80, 127.27, 124.04, 75.64, 51.20, 46.26 **MS-ESI: *m/z:*** 437.

12. (4-Benzhydrylpiperazin-1-yl)(phenyl)methanone [32]

Yield 82%; **^{1}H NMR** (400 MHz, $CDCl_3$, and TMS = 0) δ: 2.32 (2H, b), 2.48 (2H, b), 3.41 (2H, b), 3.78 (2H, b), 4.25 (1H, s), 7.15–7.19 (2H, m), 7.24–7.28 (4H, m), 7.34–7.37 (5H, m), 7.39–7.41 (4H, m); **^{13}C NMR** (100 MHz, $CDCl_3$, and TMS = 0) δ: 170.23, 142.14, 135.87, 129.60, 128.64, 128.41, 127.87, 127.20, 127.03, 76.04, 52.27, 51.71, 48.00. **MS-ESI: *m/z:*** 356.

13. (4-Benzhydrylpiperazin-1-yl)(4-nitrophenyl)methanone

Yield 75%; mp 213–215 °C, **^{1}H NMR** (400 MHz, $CDCl_3$, and TMS = 0) δ: 2.34 (2H, b), 2.51 (2H, b), 3.36 (2H, b), 3.81 (2H, b), 4.27 (1H, s), 7.17–7.20 (2H, m), 7.25–7.29 (4H, m), 7.39–7.41 (4H, m), 7.52–7.55 (2H, m), 8.22–8.25 (2H, m); **^{13}C NMR** (100 MHz, $CDCl_3$, and TMS = 0) δ:172.83, 167.81, 148.24, 141.93, 141.78, 131.72, 128.67, 128.05, 127.79, 127.28, 124.15, 123.80, 123.48, 75.87, 52.06, 51.47, 47.84, 42.39. **MS-ESI: *m/z:*** 401.

4.2.2. General procedure for synthesis of piperazine derivatives from 14 to 21

In 15 mL round bottom vial 1-substituted piperazine (0.01 mmol, 1 eq.), palladium acetate (0.1 mol%), BINAP (0.2 mol%), sodium *tert*-butoxide (0.015 mmol, 1.5 eq.) and aryl halide (0.01 mmol, 1 eq.) was taken in dry toluene (8 mL) under nitrogen environment. The reaction was kept for stirring at 110 °C in the closed vessel in silicon oil bath. Completion of reaction was confirmed by TLC. Water was added and the reaction mixture was extracted using ethyl acetate. The organic layer was dried over sodium sulphate and evaporated over rota-evaporator. Further, product was purified using column chromatography on silica gel (60–120).

14. 1,4-Diphenylpiperazine [33]

Yield 42%; **^{1}H NMR** (400 MHz, $CDCl_3$, and TMS = 0) δ: 3.37 (8H, s), 6.91 (2H, m), 7.01 (4H, m), 7.26 (4H, m); **^{13}C NMR** (100 MHz, $CDCl_3$, and TMS = 0) δ: 129.38, 116.63, 49.58, 31.11 **ESI-MS *m/z***: 238.

15. 3-(4-Phenylpiperazin-1-yl)quinolone

Yield 68%; **^{1}H NMR** (400 MHz, $CDCl_3$, and TMS = 0) δ: 2.61–2.77 (4H, m), 3.36–3.38 (4H, m), 3.47 (4H, t, *J* = 8 Hz), 7.26 (3H, m), 7.35 (1H, d, *J* = 4 Hz), 7.46 (4H, m), 7.48 (1H, d, *J* = 4 Hz), 7.98 (1H, d, *J* = 8 Hz), 8.79 (1H, bd); **^{13}C NMR** (100 MHz, $CDCl_3$, and TMS = 0) δ:145.11, 143.01, 128.99, 127.14, 126.76, 126.70, 117.76, 54.83, 49.06 **ESI-MS *m/z*:** 289.

16. 1-(Naphthalen-1-yl)-4-phenylpiperazine

Yield 43%; **IR (KBr cm^{-1})**: 1116.36(CN stretch), 2944 (CH stretch), 1030.98 (CC stretch) 1830.10 (C=C stretch) **^{1}H NMR** (400 MHz, $CDCl_3$, TMS = 0) δ: 3.34(4H, s), 3.52 (4H, s), 6.97 (1H, bd), 7.16 (1H, d, *J* = 4 Hz), 7.26 (2H, m), 7.35 (2H, m), 7.43–7.46 (1H, m), 7.49 (2H, m), 7.59 (1H, d, 8 Hz), 7.84 (1H, d, 8 Hz), 8.23 (1H, d, *J* = 8 Hz); **^{13}C NMR** (100 MHz, $CDCl_3$, and TMS = 0) δ: 134.87, 129.51, 128.63, 126.06, 126.01, 125.68, 124.04, 123.46, 115.01, 114.98, 52.90, 50.0 **ESI-MS *m/z***: 288.

17. 1-Benzhydryl-4-benzylpiperazine [33,34]

Yield 87%; **^{1}H NMR** (400 MHz, $CDCl_3$, TMS = 0) δ: 2.35–2.42 (8H, b), 3.47 (2H, s), 4.14 (1H, s), 7.05–7.09 (2H, m), 7.14–7.18 (5H, m), 7.20–7.22 (4H, m), 7.30–7.32 (4H, m); **^{13}C NMR** (100 MHz, $CDCl_3$, TMS = 0) δ: 142.76, 129.43, 128.44, 128.20, 127.94, 127.67, 127.13, 126.88, 76.19, 62.89, 53.19, 51.71. **MS-ESI: *m/z:*** 342.

18. 1-Benzhydryl-4-phenylpiperazine

Yield 95%; mp 119–120 °C, **^{1}H NMR** (400 MHz, $CDCl_3$, TMS = 0) δ: 2.55 (4H, t, *J* = 5 Hz), 3.18 (4H, t, *J* = 5 Hz), 4.25 (1H, s), 6.83 (1H, t,

J = 8 Hz), 6.88–6.90 (2H, m), 7.16–7.30 (8H, m), 7.44–7.47 (4H, m); **^{13}C NMR**(100 MHz, $CDCl_3$, and TMS = 0) δ: 151.35, 142.71, 129.12, 128.59, 127.95, 127.05, 119.53, 115.84, 76.30, 52.01, 49.23. **HRMS:** for $C_{23}H_{24}N_2$, calculated $[M+H]^+$: 329.2018; observed $[M+H]^+$: 329.2102.

19. 4-(4-Benzhydrylpiperazin-1-yl)quinoline

Yield 94%; mp 151–153 °C, **^{1}H NMR** (400 MHz, $CDCl_3$, TMS = 0) δ: 2.63 (4H, t, *J* = 5 Hz), 3.32 (4H, t, *J* = 5 Hz), 4.31 (1H, s), 7.18–7.22 (2H, m), 7.28–7.32 (5H, m), 7.42–7.51 (6H, m), 7.64–7.66 (1H, m), 7.97 (1H, d, *J* = 8 Hz), 8.77 (1H, s); **^{13}C NMR** (100 MHz, $CDCl_3$, and TMS = 0) δ: 144.87, 144.73, 142.79, 142.43, 128.88, 128.64, 127.92, 127.16, 126.91, 126.59, 126.32, 116.52, 76.15, 51.67, 49.32; **HRMS:** for $C_{26}H_{25}N_3$, calculated $[M+H]^+$: 380.2127; observed $[M+H]^+$: 380.2109.

20. 1-(Anthracen-9-yl)-4-benzhydrylpiperazine

Yield 94%; mp 185–187 °C, **^{1}H NMR** (400 MHz, $CDCl_3$, TMS = 0) δ: 2.72 (4H, t, *J* = 4 Hz), 3.54 (4H, t, *J* = 4 Hz), 4.42 (1H, s), 7.18–7.22 (2H, m), 7.29–7.33 (4H, m), 7.40–7.48 (4H, m), 7.54–7.56 (4H, m), 7.97 (2H, d, *J* = 8 Hz), 8.27 (1H, s), 8.54 (2H, d, *J* = 8 Hz); **^{13}C NMR** (100 MHz, $CDCl_3$, and TMS = 0) δ: 144.34, 143.08, 132.57, 130.62, 128.92, 128.61, 128.11, 127.01, 125.09, 124.98, 124.96, 124.86, 76.75, 53.75, 51.85. **MS-ESI: *m/z:*** 428.

21. 1-Benzhydryl-4-(naphthalen-1-yl)piperazine

Yield 90%; mp-123–124 °C, **^{1}H NMR** (400 MHz, $CDCl_3$, TMS = 0) δ: 2.68 (4H, b), 3.14 (4H, b), 4.36 (1H, s), 7.07–7.09 (1H, m), 7.17–7.23 (2H, m), 7.27–7.31 (4H, m), 7.36–7.44 (3H, m), 7.47–7.53 (5H, m), 7.78–7.80 (1H, m), 8.14–8.16 (1H, m); **^{13}C NMR**(100 MHz, $CDCl_3$, and TMS = 0) δ: 149.74, 142.82, 134.74, 128.89, 128.58, 128.39, 128.04, 127.03, 125.91, 125.79, 125.26, 123.69, 123.35, 114.51, 76.58, 53.22, 52.63. **HRMS:** for $C_{27}H_{26}N_2$, calculated $[M+H]^+$: 379.2174; observed $[M+H]^+$: 379.2161.

4.3. Biological studies

4.3.1. Determination of hMAO inhibition activity

The effects of the test compounds on hMAO enzyme were evaluated by using fluorimetric method using Amplex® Red assay kit [18].

Briefly, 100 μL of sodium phosphate buffer (0.05 M, pH 7.4) containing the synthesized test drugs and reference inhibitors, in various concentrations along with adequate amounts of recombinant hMAO (hMAO-A: 1.1 μg protein; specific activity: 150 nmol of p-tyramine oxidized to p-hydroxyphenylacetaldehyde/min/mg protein; hMAO-B: 7.5 μg protein; specific activity: 22 nmol of p-tyramine transformed/min/mg protein) enzyme, were incubated for 15 min at 37 °C in a flat-black-bottom 96-well plate (Tarsons) in incubator. After this incubation period, the reaction was started by adding (final concentrations) 200 μM Amplex® Red reagent, 1 U/mL horseradish peroxidase and 1 mM p-tyramine. After 30 min incubation in the dark, the production of H_2O_2 was quantified at 37 °C in a multi-detection microplate fluorescence reader (Synergy^{HI}, Bio-Tek® Instruments) based on the fluorescence generated at the excitation wavelength of 545 nm, and emission wavelength of 590 nm. Control experiments were carried out simultaneously by replacing the test drugs with the vehicle. To minimize the possibility of any interference of test drugs to the non-enzymatic fluorescence generated through drug and Amplex® Red reagent interactions blank reading was taken with drug and Amplex® Red reagent without adding MAO enzyme in a sodium phosphate buffer. No fluorescence could be observed in the absence of MAO enzyme thus eliminating the possibility of any false reading. The specific final fluorescence emission was calculated after subtraction of the background activity, determined from vials containing all components except the hMAO enzyme replaced by a sodium phosphate buffer solution.

4.3.2. Reversibility studies

For reversibility studies, dilution protocol was adopted as reported in the literature [19,20]. Briefly, the test inhibitors were incubated with the MAO enzymes at concentrations of 10 × IC_{50} and 100 × IC_{50} at 37 °C for of 30 min (negative control performed in the absence of inhibitor), and 4% DMSO was added as co-solvent to all incubations. After 30 min incubation period, the samples were subsequently diluted to 100–fold with the addition of tyramine substrate to achieve final inhibitor concentrations of 0. 1 × IC_{50} and 1 × IC_{50} value, respectively. As positive controls, MAO-A and MAO-B were incubated with the irreversible inhibitors, clorgyline and pargyline respectively, at 10 × IC_{50} concentrations and then diluted 100-fold to achieve final inhibitor concentrations of 0.1 × IC_{50}. The residual MAO activities after dilutions were measured (n = 3) and the residual enzyme activities were expressed as mean ± SD.

4.3.3. ROS inhibition studies

Intracellular levels of ROS were determined by using the protocol described elsewhere [35], using non-fluorescent compound 2,7-dichlorofluorescein diacetate (DCF-DA) that is permeable to the cell membrane where it is hydrolyzed by intracellular esterases and oxidized by ROS to a fluorescent compound 2,7-DCF. Cells (SH-SY5Y) were seeded in 96 well plates ($1X10^4$ cells/ well) and left for 24 h in complete media at 37 °C. The media was removed, washed with PBS and cells were treated with test compounds (without FBS) for 24 h and 48 h at different concentrations (0.1 μM and 10 μM). Thereafter, cells were rinsed with PBS three times and treated with H_2DCF-DA (50 μM) and incubated for 30 min at 37 °C. Following incubation, cells were rinsed with PBS and fluorescence was detected at a wavelength of 478 nm excitation and 518 nm emission.

4.3.4. Cytotoxicity studies

With an aim to test the cytotoxicity of the synthesized compounds on neuronal cells, MTT assays were carried out with human neuroblastoma SH-SY5Y and IMR-32 cell lines. Approximately 10,000 cells were seeded per well of 96 well plate in DMEM/F-12 media containing 10% FBS and horse serum supplemented 1% penicillin antibiotic solution for 24 h and treated as indicated in the experimental design. Cells were treated with synthesized compounds at concentration of 25 μM for 24 h and 48 h in humidified CO_2 incubator, maintained at 37 °C with 5% CO_2 and 95% humidity under serum-free conditions.

4.3.5. Molecular docking studies

To determine the mode of interaction between synthesized ligands and the active site of hMAO-A and hMAO-B enzymes, molecular docking studies were performed using Glide [36] module of Maestro 11.1 (Schrödinger LLC). X-ray crystal structures of hMAO-A (PDB ID- 2BXR) and hMAO-B (PDB ID- 2BYB) [23] enzymes were imported from the protein data bank (www.rscb.org). Protein was prepared using "protein preparation wizard" application of Schrödinger suite 2017. The energy was minimized using an OPLS2005 force field. The grid was generated (20 Å) around the co-crystallized ligand using receptor grid generation module of Maestro 11.1. Ligands were drawn in ChemBio Draw Ultra-12 and prepared using ligand preparation application in Schrödinger suite 2017. For each compound, the top-score docking poses were chosen for final ligand-target interaction analysis employing XP interaction visualizer of Maestro 11.1 software. Validation of docking procedure was first evaluated by re-docking of the co-crystalized ligand into the active site of MAO enzyme. Qikprop [37,38] application of Schrodinger suit was used to determine the drug like and ADME properties of the compounds.

4.3.6. MD simulation studies

In order to investigate the behavior of test inhibitors in the active site of the MAO, molecular dynamic (MD) simulation was performed. The docking complex of compound 12 with the active cavity of MAO-B was used. MD simulations were performed using Desmond [39,40]. Complex was solvated by TIP3P water model and then naturalized by adding 0.15 M Na^+ and Cl^- ions. The thickness of water layer was set to 10 Å. Before the MD simulations the systems were minimized with a maximum iteration of 2000 steps. Then, the systems were submitted to 30 ns MD simulation for equilibration and production MD run. Temperature and pressure were assigned at 300 K and 1.01325 bar, respectively using Isothermal–isobaric (NPT) ensemble. Cut-off radios of 9 Å was used for Coulomb interactions.

Acknowledgement

V.K. is thankful to the University Grant Commission (UGC), New Delhi, India for providing the financial assistance (BSR Grant NO. F.20-17(12)/2012). BK is thankful to CUP, Bathinda and UGC for PhD fellowship.

Conflict of interest

The authors indicate no potential conflicts of interest.

Appendix A. Supplementary material

Supplementary data associated with this article can be found, in the online version, at https://doi.org/10.1016/j.bioorg.2018.01.020.

References

[1] L. Santana, E. Uriarte, H. González-Díaz, G. Zagotto, R. Soto-Otero, E. Méndez-Álvarez, A QSAR model for in silico screening of MAO-A inhibitors. Prediction, synthesis, and biological assay of novel coumarins, J. Med. Chem. 49 (2006) 1149–1156.
[2] M. Catto, O. Nicolotti, F. Leonetti, A. Carotti, A.D. Favia, R. Soto-Otero, E. Méndez-Álvarez, A. Carotti, Structural insights into monoamine oxidase inhibitory potency and selectivity of 7-substituted coumarins from ligand- and target-based approaches, J. Med. Chem. 49 (2006) 4912–4925.
[3] S. Carradori, M. D'Ascenzio, C. De Monte, D. Secci, M. Yanez, Synthesis and selective human monoamine oxidase B inhibition of heterocyclic hybrids based on hydrazine and thiazole scaffolds, Arch. Pharm. 346 (2013) 17–22.
[4] L. Novaroli, A. Daina, E. Favre, J. Bravo, A. Carotti, F. Leonetti, M. Catto, P.-A. Carrupt, M. Reist, Impact of species-dependent differences on screening, design, and development of MAO B inhibitors, J. Med. Chem. 49 (2006) 6264–6272.
[5] J.A. Morón, M. Campillo, V. Perez, M. Unzeta, L. Pardo, Molecular determinants of MAO selectivity in a series of indolylmethylamine derivatives: biological activities, 3D-QSAR/CoMFA analysis, and computational simulation of ligand recognition, J. Med. Chem. 43 (2000) 1684–1691.
[6] P. Ganrot, E. Rosengren, C. Gottfries, Effect of iproniazid on monoamines and monoamine oxidase in human brain, Cell Mol. Life Sci. 18 (1962) 260–261.
[7] A. Cooper, Tyramine and irreversible monoamine oxidase inhibitors in clinical practice, Brit. J. Psychiat., 1989.
[8] M.E. Thase, M.H. Trivedi, A.J. Rush, MAOIs in the contemporary treatment of depression, Neuropsychopharmacol. 12 (1995) 185–219.
[9] B. Kumar, A.K. Mantha, V. Kumar, Recent developments on the structure–activity relationship studies of MAO inhibitors and their role in different neurological disorders, RSC Adv. 6 (2016) 42660–42683.
[10] B. Kumar, V. Prakash Gupta, V. Kumar, A perspective on monoamine oxidase enzyme as drug target: challenges and opportunities, Curr. Drug Target. 18 (2017) 87–97.
[11] M. Youdim, M. Fridkin, H. Zheng, Novel bifunctional drugs targeting monoamine oxidase inhibition and iron chelation as an approach to neuroprotection in Parkinson's disease and other neurodegenerative diseases, J. Neural Transm. 111 (2004) 1455–1471.
[12] H. Zheng, S. Gal, L.M. Weiner, O. Bar-Am, A. Warshawsky, M. Fridkin, M.B. Youdim, Novel multifunctional neuroprotective iron chelator-monoamine oxidase inhibitor drugs for neurodegenerative diseases: in vitro studies on antioxidant activity, prevention of lipid peroxide formation and monoamine oxidase inhibition, J. Neurochem. 95 (2005) 68–78.
[13] C. Meher, A. Rao, M. Omar, Piperazine-pyrazine and their multiple biological activities, Asian J. Pharm. Sci. Res. 3 (2013) 43–60.
[14] A.L. Johnstone, G.W. Reierson, R.P. Smith, J.L. Goldberg, V.P. Lemmon, J.L. Bixby, A chemical genetic approach identifies piperazine antipsychotics as promoters of CNS neurite growth on inhibitory substrates, Mol. Cell Neurosci. 50 (2012) 125–135.
[15] H. Pessoa-Mahana, G.R. Gajardo, R. Araya-Maturana, J.K. Cárcamo, C.D. Pessoa-Mahana, Synthesis of 4-Arylpiperazine derivatives of moclobemide: potential antidepressants with a dual mode of action, Synth. Commun. 34 (2004) 2513–2521.
[16] F. Pettersson, P. Svensson, S. Waters, N. Waters, C. Sonesson, Synthesis and evaluation of a set of para-substituted 4-phenylpiperidines and 4-phenylpiperazines as monoamine oxidase (MAO) inhibitors, J. Med. Chem. 55 (2012) 3242–3249.
[17] F. Pettersson, P. Svensson, S. Waters, N. Waters, C. Sonesson, Synthesis, pharmacological evaluation and QSAR modeling of mono-substituted 4-phenylpiperidines and 4-phenylpiperazines, Eur. J. Med. Chem. 62 (2013) 241–255.
[18] F. Chimenti, S. Carradori, D. Secci, A. Bolasco, B. Bizzarri, P. Chimenti, A. Granese, M. Yanez, F. Orallo, Synthesis and inhibitory activity against human monoamine oxidase of N1-thiocarbamoyl-3, 5-di (hetero) aryl-4, 5-dihydro-(1H)-pyrazole derivatives, Eur. J. Med. Chem. 45 (2010) 800–804.
[19] S. Mostert, W. Mentz, A. Petzer, J.J. Bergh, J.P. Petzer, Inhibition of monoamine oxidase by 8-[(phenylethyl) sulfanyl] caffeine analogues, Bioorg. Med. Chem. 20 (2012) 7040–7050.
[20] C. Minders, J.P. Petzer, A. Petzer, A.C. Lourens, Monoamine oxidase inhibitory activities of heterocyclic chalcones, Bioorg. Med. Chem. 25 (2015) 5270–5276.
[21] N. Pizzinat, N. Copin, C. Vindis, A. Parini, C. Cambon, Reactive oxygen species production by monoamine oxidases in intact cells, Naunyn Schmiedebergs Arch. Pharmacol. 359 (1999) 428–431.
[22] A. Sturza, L. Noveanu, O. Duicu, D. Angoulvant, D.M. Muntean, 0209: Monoamine oxidases as novel sources of reactive oxygen species in experimental diabetes, Arch. Cardiovasc. Dis. Supple. 6 (2014) 15.
[23] L. De Colibus, M. Li, C. Binda, A. Lustig, D.E. Edmondson, A. Mattevi, Three-dimensional structure of human monoamine oxidase A (MAO A): relation to the structures of rat MAO A and human MAO B, Proc. Natl. Acad. Sci. USA 102 (2005) 12684–12689.
[24] T. Irikura, K. Masuzawa, K. Nishino, M. Kitagawa, H. Uchida, N. Ichinoseki, M. Ito, New analgetic agents. V. 1-Butyryl-4-cinnamylpiperazine hydrochloride and related compounds, J. Med. Chem. 11 (1968) 801–804.
[25] X. He, A. Alian, P.R.O. de Montellano, Inhibition of the Mycobacterium tuberculosis enoyl acyl carrier protein reductase InhA by arylamides, Bioorg. Med. Chem. 15 (2007) 6649–6658.
[26] M.S. Yu, D.P. Curran, T. Nagashima, Increasing fluorous partition coefficients by solvent tuning, Org. Lett. 7 (2005) 3677–3680.
[27] R.N. Prasad, L.R. Hawkins, K. Tietje, Potential antihypertensive agents. II. Unsymmetrically 1,4-disubstituted piperazines. 1, J. Med. Chem. 11 (1968) 1144–1150.
[28] J. Tong, Y. Chen, S. Liu, X. Xu, QSAR studies of antituberculosis drug using three-dimensional structure descriptors, Med. Chem. Res. 22 (2013) 4946–4952.
[29] C.A. Kumar, S.N. Swamy, N. Thimmegowda, S.B. Prasad, G.W. Yip, K. Rangappa, Synthesis and evaluation of 1-benzhydryl-sulfonyl-piperazine derivatives as inhibitors of MDA-MB-231 human breast cancer cell proliferation, Med. Chem. Res. 16 (2007) 179–187.
[30] S. Naveen, C.A. Kumar, S.B. Prasad, K. Vinaya, M. Sridhar, J.S. Prasad, K. Rangappa, Structural conformation of a novel 1-benzhydrylpiperazine derivative: 1-benzhydryl-4-(toluene-4-sulfonyl)-piperazine, J. Chem. Crystallogr. 39 (2009) 395–398.
[31] K. Vinaya, S. Naveen, C.A. Kumar, S. Benakaprasad, M. Sridhar, J.S. Prasad, K. Rangappa, Synthesis, characterization, crystal and molecular structure analysis of a novel 1-benzhydryl piperazine derivative: 1-benzhydryl-4-(2-nitro-benzenesulfonyl)-piperazine, Struct. Chem. 19 (2008) 765–770.
[32] M. Rotta, K. Pissinate, A.D. Villela, D.F. Back, L.F.S.M. Timmers, J.F.R. Bachega, O.N. de Souza, D.S. Santos, L.A. Basso, P. Machado, Piperazine derivatives: synthesis, inhibition of the Mycobacterium tuberculosis enoyl-acyl carrier protein reductase and SAR studies, Eur. J. Med. Chem. 90 (2015) 436–447.
[33] J.P. Safko, R.D. Pike, Synthesis and crystal structures of N,N′-disubstituted piperazines, J. Chem. Crystallogr. 42 (2012) 981–987.
[34] H. Ohtaka, T. Kanazawa, K. Ito, G. Tsukamoto, Benzylpiperazine derivatives. IV Syntheses and cerebral vasodilating activities of 1-benzyl-4-diphenylmethylpiperazine derivatives, Chem. Pharm. Bull. 35 (1987) 3270–3275.
[35] N. Kaur, M. Dhiman, J.R. Perez-Polo, A.K. Mantha, Ginkgolide B revamps neuroprotective role of apurinic/apyrimidinic endonuclease 1 and mitochondrial oxidative phosphorylation against Aβ25–35-induced neurotoxicity in human neuroblastoma cells, J Neurosci. Res. 93 (2015) 938–947.
[36] R.A. Friesner, J.L. Banks, R.B. Murphy, T.A. Halgren, J.J. Klicic, D.T. Mainz, M.P. Repasky, E.H. Knoll, M. Shelley, J.K. Perry, D.E. Shaw, Glide: a new approach for rapid, accurate docking and scoring. 1. Method and assessment of docking accuracy, J. Med. Chem. 47 (2004) 1739–1749.

[37] L.L.C. Schrödinger, "QikProp, version 3.5." New York, NY, 2012.
[38] B. Kumar, M. Kumar, A.R. Dwivedi, V. Kumar, Synthesis, Biological Evaluation and Molecular Modeling Studies of Propargyl Containing New 2,4,6-trisubstituted Pyrimidine Derivatives as Potential anti-Parkinson agents. ChemMedChem. 10.1002/cmdc.201700589 in press.
[39] Desmond Molecular Dynamics System, Version 2.2 D.E. Shaw Research, New York, NY, 2009.
[40] M. Singh, O. Silakari, Design, synthesis and biological evaluation of novel 2-phenyl-1-benzopyran-4-one derivatives as potential poly-functional anti-Alzheimer's agents, RSC Adv. 6 (2016) 108411–108422.